Argus Finger: Optical Multimode-Sensing Skin for Gripper Fingers
The Prototype and A Demonstration in Cutting Vegetables

Akihiko Yamaguchi[1] and Christopher G. Atkeson[1]

***Abstract*— *WRITE HERE* Argus Finger: Optical Multimode-Sensing Skin for Gripper Fingers The Prototype and A Demonstration in Cutting Vegetables**

Multimodal Optical See-through Soft Sensing Skin Optical Multimode-Sensing Skin

I. Introduction

We are exploring a whole-body vision as a sensing skin for the human-safe efficient robot control. Different types of sensors are useful to maintain the human safety, such as proximity sensors and contact sensors. Those sensors are also useful in robust robot control. For example in the DARPA robotics challenge finals, no robots are using railings, walls, door frames, or environment obstacles to support the robot body [1]. In order to achieve such a multi-contact motion control, whole-body contact sensors are important. We are proposing to cover the robot body with a transparent soft material (skin) and put cameras inside. Such a whole-body vision will give us multimodal information such as a proximity (by a stereo vision), visual information (color, texture), and a contact force estimation (by detecting the skin deformation). This project is named "Argus Project"; Argus Panoptes is a 100-eyed giant in Greek mythology.

This paper focuses on such a sensing skin for robotic grippers. We design the sensing skin for manipulation tasks more than grasping. Especially we consider a cutting task with a knife. During cutting, sometimes a strong force is applied to the knife when cutting a hard material, which causes the knife slippage or the damage to the fingers. We intend to make a sensing skin that is useful for such a situation; contact force estimations for avoiding the slippage and the damage to the fingers, and visual information for the slippage detection.

There are many similar approaches to make a tactile sensor with a transparent skin and an imaging sensor inside (e.g. [2], [3], [4], [5], [6], [7]), but all of them are focusing on the tactile sensing only, i.e. contact point location and/or contact force/pressure. Most of them are covering the skin surface with opaque material to shut out the external light. We think the see-through skin gives us richer information.

In this paper, we make a prototype of the sensing skin. It consists of a camera, a transparent hard layer made with acrylic, a transparent soft layer made with silicone rubber, and colored markers embedded around the surface of the soft layer. The markers are used to make the skin-deformation detection easy. A computer vision method is developed for tracking the markers in order to estimate contact forces. We integrate the sensing skin to the gripper of a Baxter robot, and investigate its usefulness in a practical situation, cutting vegetables with a knife.

Our sensing skin has good features. It is comparably low cost; it just uses the off-the-shelf materials. It is easy to make. The issue is the reduction. The bottle necks are cameras and lenses. Recently small cameras are widely developed for various purposes including smart phones, so we think this issue will be gradually solved. For example in [8], a human fingertip-size device was made with a tiny camera. Our sensing skin is useful; it gives us higher resolution of contact forces and proximity vision. It is physically robust because the sensor is separated from the skin. We assume that the sensing skin is installed on a robot by fixing the hard layer on a rigid part of the robot. Thus the external force is applied to the soft and hard layers only.

Related Work

The idea of using imaging sensors for tactile sensing is researched from some decades ago. An initial attempt was measuring the frustration of total internal reflection within a waveguide on sensor surface caused by contact [2], [3]. The research trend has been shifted to measuring displacement of markers located on the sensor surface with computer vision [4], [5], [6], [7]. A reason would be the marker displacements correspond with the external force as the displacements are directly caused by the external force. The resolution of the contact force array is decided by the camera and the marker density. Recently a high resolution sensor is proposed [7]. Many of these researches use a transparent elastic material between the sensor surface and the base. The dynamic range of the force measurement can be controlled by changing the hardness of the elastic material (softer is more sensitive; cf. [9]).

Our research is following this approach. An important difference is the transparency of the skin, which gives us richer and multi-modal information. The above researches use opaque surfaces to block the external light as it would affect the marker tracking. We attempt to solve the marker tracking problem in natural external scenes in order to make use of the transparent skin.

Many of similar researches are using a hemisphere shape for fingertip [3], [5], [6], [7], [9]. They attempted to make fingertips of robotic hands or grippers. The surface shape is decided by tasks of the robotic grippers. Although there are researches of the other shapes such as a flat shape (e.g. [2],

[1]A. Yamaguchi and C. G. Atkeson are with The Robotics Institute, Carnegie Mellon University, 5000 Forbes Avenue, Pittsburgh PA 15213, United States info@akihikoy.net

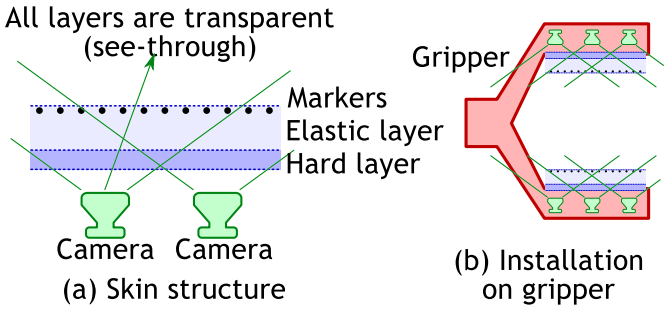

Fig. 1. Conceptual design of our optical multimode-sensing skin and the installation example on a robotic gripper.

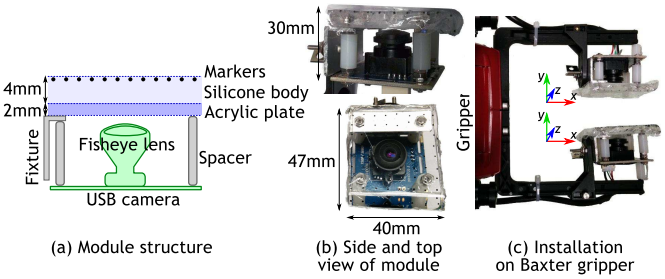

Fig. 2. Prototype module of the optical multimode-sensing skin (a,b) and its installation on the Baxter gripper.

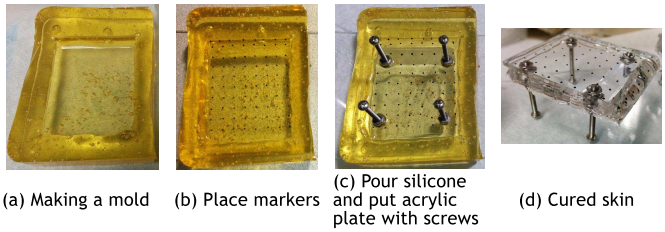

Fig. 3. Process of making the see-through skin.

[4]), the surface shape requirements have not been researched enough in the context of application tasks. We explore a flat surface and show the usefulness in a cutting task.

II. Optical Multimode-Sensing Skin for Robot Finger

A. Overview

The conceptual design of the optical multimode-sensing skin is shown in Fig. 1. Unlike to other researches [4], [6], [7], we do not place an opaque material on the surface. The whole skin is transparent except for markers, and the cameras can see the external scene through the skin.

The markers are captured by the cameras and tracked by an image processing, that gives us a 3-axis (x,y,z) force-relevant measurement of each marker point. By combining multiple marker measurements, we can estimate torque-relevant information. In general, a bigger marker is easier to detect; the marker size affects the accuracy of tracking. The density of the markers decides the resolution of the contact force array. There is a trade-off between the resolution and the surface transparency. The hardness and the thickness of the elastic layer affect the marker movement caused by contact force (softer layer is easily deformed by a small force). They decide the dynamic range of the contact force measurement. The hard layer is assumed to be fixed on the gripper so that the external force is applied to elastic and hard layers only and does not affect the cameras. Thus the physical robustness of the sensing skin is decided by the elastic and the hard layers. The camera resolution affects the accuracy of the marker detection and tracking. The camera frame rate affects the sensing frame rate. These properties (the marker size and density, the hardness and the thickness of the elastic and hard layers, and the camera property) are decided by the purpose (task) of each part of the skin.

B. Prototype Module of Optical Multimode-Sensing Skin

We make a prototype module of the optical multimode-sensing skin for the parallel gripper of a Baxter robot. For simplicity, we use one camera for each finger.

Fig. 2 shows the prototype module and its installation on the Baxter gripper. The size of the module is about 40 mm (W) x 47 mm (L) x 30 mm (H) including a camera module with a USB interface. In the following, we describe the detail of making the module.

1) See-through Skin with Markers: Fig. 3 shows a process to make the see-through skin with markers. First we make a mold for the elastic layer. The fingertip edge has a rounded shape; the other part is flat. Then we put markers on the bottom of the mold. As the markers, we use micro plastic beads of black color, that are spheres of around 1 mm diameter. The markers are placed on a grid whose interval is around 5 mm. We pour silicone rubber into the mold. As the silicone, we use Silicones Inc. XP-565 that has A-16 shore hardness after cure. Degassing silicone was important to keep the transparency before pouring the silicone into the mold. Right after pouring into the silicone, we put an acrylic plate (40 mm x 40 mm, 2 mm thickness) with screws as shown in Fig. 3(c). These screws are for preventing the acrylic plate sinking into the silicone, and creating a space for screw heads when attaching the skin to the camera. The thickness of the silicone layer is 4 mm. Fig. 3(d) shows the silicone layer with the acrylic plate after curing. Finally we cover the skin with a thin transparent plastic film to protect the silicone skin from dirt. This film is replaceable.

2) Skin on Camera: We attach the skin on the camera. The camera is ELP co. USBFHD01M-L180 which is an RGB camera with a USB interface and a 180 degree fisheye lens. Thus, this skin module works as a stand-alone USB sensor. The lens is adjusted to focus on the markers, which improves the marker tracking quality. When attaching the skin on the camera, we embed a fixture used for integrating into the Baxter gripper. The fixture is a L-shaped aluminum plate whose one edge is fixed on the acrylic plate (see Fig. 2(a)). Fig. 2(b) shows the side and top views of the module. In the top view, we can see the camera through the skin; thus the

silicone and acrylic layers have good transparency.

C. Installation to Gripper Fingers of Baxter Robot

The gripper of the Baxter robot is a parallel gripper with two fingers. We made two prototype modules and attach one for each finger. We create a simple mount for the sensor as shown in Fig. 2(c).

D. Marker Tracking for Contact Force Estimation

As the marker detection, we use an existing blob detection method implemented in OpenCV[1], `cv::SimpleBlobDetector`, that detects small blobs from an image. Each detected blob has the position (x,y) and the size on the image.

Since the camera image is distorted due to the fisheye lens, we rectify the input image before detecting the blobs. We use calibration methods in OpenCV.

Our marker tracking algorithm is simple. First we calibrate the marker tracker by obtaining the initial marker positions and sizes. In each frame, we compare the current marker positions and sizes with the initial markers. The details are described in following.

1) Marker tracker calibration: We use 20 frames for the marker tracker calibration where we put a white board on the skin so that the blob detector detects only the markers. If there are moving blobs, they are considered as outliers. We take an average of the remaining blob positions and sizes and keep them as the initial markers.

2) Marker tracking: In each frame, we detect blobs from an input image, and compare them with the initial markers. Since the order of the blobs does not correspond with the initial markers, we assume the closest blob is the same marker. We put thresholds on position and size differences, and if they are too large, we consider them as outliers. For each marker position and size differences dx, dy, ds, we estimate the contact force $\mathbf{f}$ as:

$$\mathbf{f} = [c_x dx, c_z ds, c_y dy] \tag{1}$$

where c_x, c_y, c_z are conversion coefficients (refer to Fig. 2(c) for the coordinate definition). These coefficients are for human readability, not for conversing to regular units such as Newton.

We can use these contact force estimates as a force array. We can also convert them to an average force and torque, which would be useful for simple applications. For this, first we define a torque estimate around the center of the skin surface as: $\boldsymbol{\tau} = c_\tau \mathbf{r} \times \mathbf{f}$, where $\mathbf{r}$ is a displacement vector from the center of the skin surface to the marker, and c_τ is a conversion coefficient. For averaging $\mathbf{f}$ and $\boldsymbol{\tau}$, we use the element-wise 80th percentile[2] of the absolute value. This filter gives us a robust estimation against the outliers in the marker tracking, and picks up a local force when the external force is applied to a narrow region of the skin surface.

[1] `http://opencv.org/`

[2] Using the value splitting the highest 20% of the data from the lowest 80%.

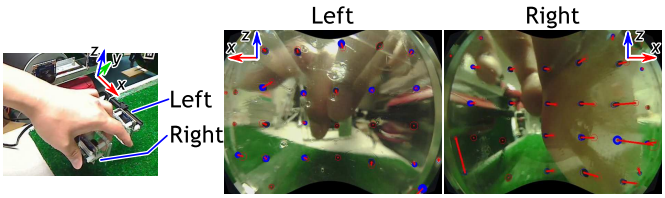

Fig. 4. Pushing force by a human subject. The right two images are views from the cameras. The marker movements are rendered (the movements are emphasized).

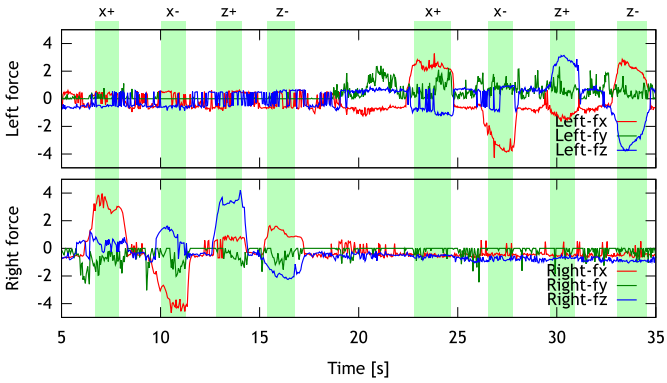

Fig. 5. Trajectories of the average force (x,y,z) of the left (top graph) and the right (bottom graph) sensing skins during pushing by a human subject.

We programmed the above methods with as many threads as possible. The whole process including capturing from cameras is computed in around 30 frame per second with two cameras whose resolution is 640x480. The computer has an Intel Core i7 CPU (2.70 GHz, 4 cores, 8 hyper threads) processor and 16 GB RAM.

III. Experiments

We demonstrate our sensing skin in some experiments. In these experiments we do not apply a temporal filter.

A. Pushing Force Directly Applied to The Skin

First, we let a human subject to push the skin horizontally (x and z axes) for each finger respectively. Fig. 4 shows the captured image (rectified) with visualizing the marker movements during pushing. We can see that the markers are moved by fingers, and can see the fingers through the skin. Fig. 5 shows the trajectories of the average force (x,y,z) of the left and the right sensing skins. In both sides, the horizontal (x and z) forces are changing to pushed directions. During pushing, the vertical (y) force is changing slightly, but is noisy. This is because the vertical force is estimated from the marker size change and the size does not change largely compared to the horizontal marker displacement. The reason why the value of the left sensor is changing around 20 sec is that the finger of the human is contacting the skin.

B. Pushing Force Applied to Holding Knife

We make the robot hold an knife and let a human subject to push or pull the knife in various directions as shown

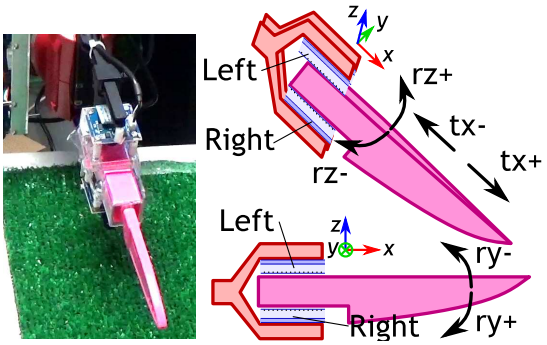

Fig. 6. Experimental setup of pushing a knife held by the gripper. Pushing directions are illustrated.

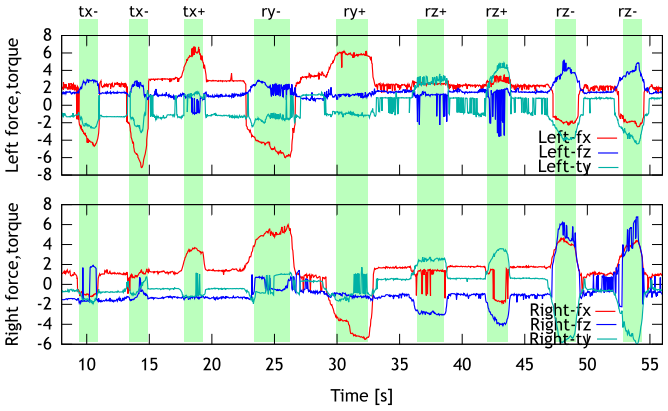

Fig. 7. Trajectories of the average force (x,z) and torque (y) of the left and the right sensing skins during pushing the knife.

in Fig. 6. Fig. 7 shows the trajectories of the average force (x,z) and torque (y) of the left and the right sensing skins. Each sensor value has an offset value since the gripper is holding the knife. The horizontal pushing (tx+, tx−) are well captured by the x-force value of the left sensor, while the second tx− (around 14 sec) is hardly detected by the right sensor. The reason would be that the surfaces of the sensors were not completely parallel due to an inaccurate construction, which probably caused an asymmetric force distribution. The vertical rotational-pushing (ry+, ry−) are detected clearly by the x-force values of the both sensor which have opposite directions because of the torque applied to the knife. Fig. 8 shows the marker tracking result in ry−. The y-torque value is capturing well the horizontal rotational-pushing (rz+, rz−), however it seems having a large hysteresis.

C. Force Profile of Cutting Motion by Human

Next, we let a human subject hold a knife with the sensing skins. For this purpose, we detach the fingers from the robot and let the human subject hold the entire finger with the knife as shown in Fig. 9. The subject cuts a banana and an apple. Fig. 10 shows the trajectories of the average force (x,z) and torque (y) of the left and the right sensing skins. The first half is cutting a banana several times, and the last half is

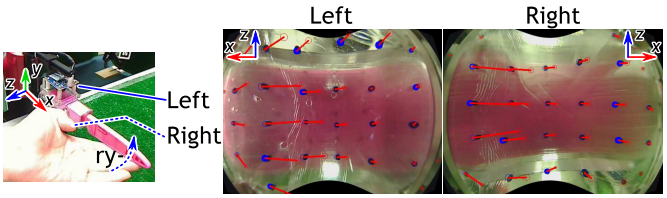

Fig. 8. Marker tracking result in pushing in the ry− direction (vertical rotation). The left image is a view from an external camera.

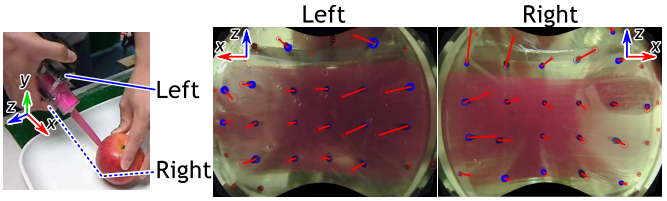

Fig. 9. Setup of the cutting motion by a human subject. The human subject holds the sensors with a knife, and cuts materials. The left view shows an example of cutting an apple, and the right two views are views of the sensing skins.

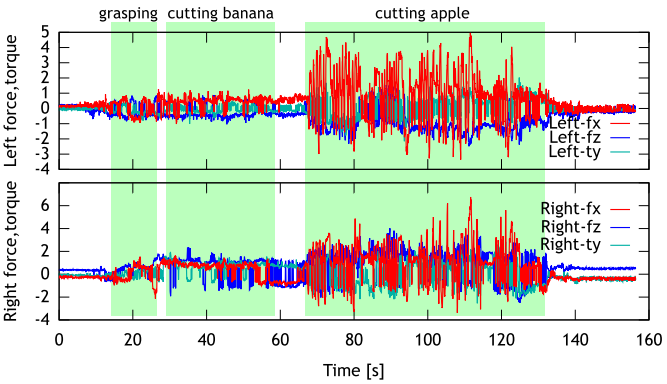

Fig. 10. Trajectories of the average force (x,z) and torque (y) of the left and the right sensing skins during cutting a banana and an apple by the human subject. In the first short period, the subject grasped the knife, and then cut the banana and the apple.

cutting an apple. There is a significant difference between cutting the apple and banana, there is subtle sensor value changes during cutting the banana because of the softness of banana. The subject was cutting the apple with waving the knife while the banana was cut by just sliding the knife. This was due to the hardness of the apple.

D. Robotic Cutting Motion with Sensing Skin

We implement a automatic cutting motion with the sensing skins. Through our preliminary experiments where we controlled the robot manually with a joy stick controller, we found difficulties: (1) When cutting a hard material, a strong vertical force is applied to the knife, which slightly deforms the gripper and the sensor mount. As the result, the knife floats from the skin (cf. Fig. 11(a)). (2) When a force is applied to the knife horizontally, the knife slips in the gripper (cf. Fig. 11(b)). In this experiment, we show that using our sensing skins, we can easily make a controller to

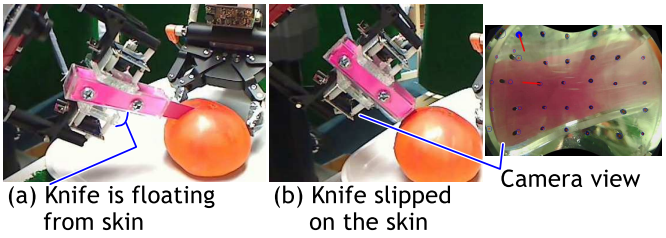

Fig. 11. Difficulties in cutting.

avoid these difficulties. Note that even if (1) or (2) happens, the visual views through the skin tell us something happened. For example, look at the camera view of Fig. 11(b); we can find that the angle of the knife is different from the initial.

We create a cutting controller which (a) starts from a state where the knife held by the gripper is put above the material, (b) moves the knife downward (cutting vertically), and then (c) slightly pulls the knife (cutting horizontally). The controller moves the knife to the initial position in order to repeat the motion several times. The difficulties (1) and (2) might happen in the step (b). To avoid them, we consider conditions to stop the motion: (A) if $-(f_{\mathrm{L}x} - f_{\mathrm{L}x0})(f_{\mathrm{R}x} - f_{\mathrm{R}x0}) > 10$, or (B) if $|\tau_{\mathrm{L}y}| + |\tau_{\mathrm{R}y}| > 4$, where $f_{\mathrm{L}x}$ and $f_{\mathrm{R}x}$ indicate the x-value of the average force of the left and the right sensors, $f_{\mathrm{L}x0}$ and $f_{\mathrm{R}x0}$ indicate their initial values (right before cutting), and $\tau_{\mathrm{L}y}$ and $\tau_{\mathrm{R}y}$ indicate the y-value of the average torque of the left and the right sensors. The condition (A) is defined according to the result of ry− in Section III-B where the vertical force was applied to the knife. The condition (B) is for avoiding the rotational knife slip.

Fig. 12 and Fig. 13 shows the sensor values during cutting a banana and an apple respectively where the trajectories of the average force (x,z) and torque (y) of the left and the right sensing skins are shown. Since the cutting a banana requires small force, the robot cut it with a single trial, while the robot repeated four times for cutting an apple. In the banana case, the robot stopped moving down the knife because the condition (A) was satisfied as the knife hit the cutting board. In the apple case, the condition (A) was satisfied by the pressure from the cut edge of the apple fresh and the cutting board. In these graphs, the condition (B) was not satisfied, but it was useful when the initial knife orientation was not perpendicular. Although the cutting motion is simple, it is capable to cut materials while avoiding the above difficulties (1), (2).

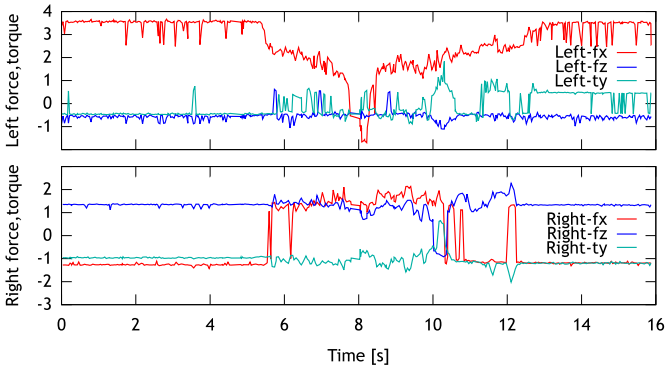

Fig. 12. Trajectories of the average force (x,z) and torque (y) of the left and the right sensing skins during cutting a banana by the robot. There was a single cutting motion around the peak of left x-force.

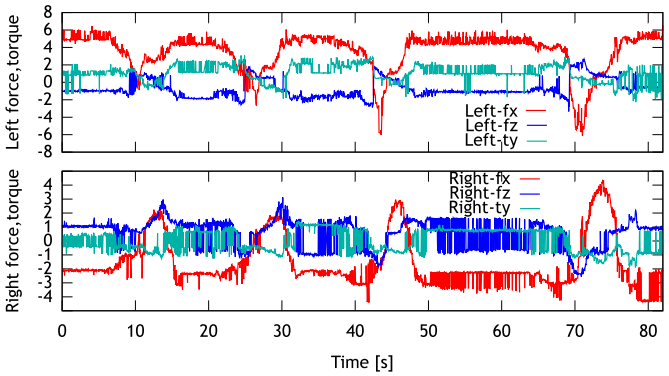

Fig. 13. Trajectories of the average force (x,z) and torque (y) of the left and the right sensing skins during cutting an apple by the robot. The robot performed the cutting motion four times to cut the apple completely. The peaks of left and right x-force correspond with the cutting motion.

IV. Discussion

1) Should we convert the force estimation to a regular unit (e.g. Newton)?: This depends on application. We are thinking to use machine learning methods to learn the dynamical models (relation between input gripper motion and output force changes) for example by using neural networks [10]. In such a case, obtaining contact force information in a regular unit is not necessary. Only the consistent estimate is important. However using a regular unit will be generalizable to other situations like other robots, so it will be still useful.

2) Accuracy, reliability, hysteresis: Although we did not conduct controlled evaluation, the horizontal force seemed to be reliable. This is because the marker movement in horizontal direction is easier to track. The vertical force seemed to be more difficult to detect as the changes of the marker size are comparably smaller. Perhaps we can use the vertical force estimate as on/off signal. A way to improve the vertical force accuracy is increasing the thickness of the elastic layer, although it would make the skin heavier.

In the experiments, there were some false detections of the markers. These were mostly due to the external light. Increasing the number of markers is helpful to reduce this, although it will reduce the transparency as well. Putting an internal light source would be helpful in dark scenes.

We found hysteresis, especially when a strong force was applied. In the cutting vegetable experiments by the robot, the force estimate changed before and after cutting a hard material. This would be because the deformation of the soft layer kept remaining. This was reset after releasing the knife.

3) Calibration frequency: During the whole experiments of the previous section, we did the calibration of the marker

tracking only twice. The first one was the initialization. The second one was necessary due to the accidental separation of the soft layer and the acrylic base.

4) Physical robustness: A weak part of the sensor is the adhesion between the soft skin and the acrylic base. Currently we rely on the sticky property of the silicone rubber. It was enough strong against the horizontal forces and downward forces from above, but the skin can be easily peeled by upward forces from below. This issue would be solved by an adhesive between the layers.

Other than that, the sensor strength is decided by the acrylic base hardness and the soft skin. For heavier tasks where larger contact forces will be applied, we would need a ticker acrylic base. Although the soft skin is weak against something with thin tips (e.g. needle) or sharp edges (e.g. knife), the hardness is close to that of the human skin. Thus we think it is enough strong for daily manipulations.

V. Conclusion

WRITE HERE

References

[1] C. Atkeson *et al.*, "NO FALLS, NO RESETS: Reliable humanoid behavior in the DARPA robotics challenge," in *the 15th IEEE-RAS International Conference on Humanoid Robots (Humanoids'15)*, 2015.

[2] S. Begej, "Planar and finger-shaped optical tactile sensors for robotic applications," *IEEE Journal on Robotics and Automation*, vol. 4, no. 5, p. 47200484, 1988.

[3] H. Maekawa, K. Tanie, K. Komoriya, M. Kaneko, C. Horiguchi, and T. Sugawara, "Development of a finger-shaped tactile sensor and its evaluation by active touch," in *Robotics and Automation, 1992. Proceedings., 1992 IEEE International Conference on*, vol. 2, 1992, pp. 1327–1334.

[4] K. Kamiyama, H. Kajimoto, N. Kawakami, and S. Tachi, "Evaluation of a vision-based tactile sensor," in *Robotics and Automation, 2004. Proceedings. ICRA '04. 2004 IEEE International Conference on*, vol. 2, 2004, pp. 1542–1547.

[5] J. Ueda, Y. Ishida, M. Kondo, and T. Ogasawara, "Development of the naist-hand with vision-based tactile fingertip sensor," in *Proceedings of the 2005 IEEE International Conference on Robotics and Automation*, 2005, pp. 2332–2337.

[6] Y. Ito, Y. Kim, and G. Obinata, "Robust slippage degree estimation based on reference update of vision-based tactile sensor," *IEEE Sensors Journal*, vol. 11, no. 9, pp. 2037–2047, 2011.

[7] N. F. Lepora and B. Ward-Cherrier, "Superresolution with an optical tactile sensor," in *Intelligent Robots and Systems (IROS), 2015 IEEE/RSJ International Conference on*, 2015, pp. 2686–2691.

[8] X.-D. Yang, T. Grossman, D. Wigdor, and G. Fitzmaurice, "Magic finger: Always-available input through finger instrumentation," in *Proceedings of the 25th Annual ACM Symposium on User Interface Software and Technology*, 2012, pp. 147–156.

[9] O. Co., "White paper: Optical force sensors — introduction to the technology," Tech. Rep., January 2015.

[10] A. Yamaguchi and C. G. Atkeson, "Neural networks and differential dynamic programming for reinforcement learning problems," in *the IEEE International Conference on Robotics and Automation (ICRA'16)*, 2016.